ENCIT 2018

ABCM Associação Brasileira de Engenharia e Ciências Mecânicas

17th Brazilian Congress of Thermal Sciences and Engineering
November 25th-28th, 2018, Águas de Lindóia, SP, Brazil

ENCIT-2018-0331
INFLUENCE OF TURBULENCE ON THE FLAMELESS COMBUSTION FLOW FIELD

Helio Henrique Santomo Villanueva
Filipi Martins Fernandes Silva
Guenther Carlos Krieger Filho
Department of Mechanical Engineering, Polytechnic School of the University of São Paulo, São Paulo, 05508-030, Brazil
heliovillanueva@usp.br, filipimfs@usp.br, guenther@usp.br

Abstract. *This paper presents a numerical study of the influence of turbulence on the flow field of the flameless combustion regime. The numerical simulations are based on experimental data in literature. Reynolds Averaged Navier-Stokes simulations using the standard k-ε model for turbulence and flamelet generated manifolds with presumed β-PDF for turbulent combustion modeling are carried out in the commercial CFD software Fluent. The numerical results agree well with main flameless regime characteristics observed experimentally and further discussion regarding the turbulent kinetic energy field, Kolmogorov time scale and Damköhler number distributions and temperature field present an objective view of the numerical models applied.*

Keywords: *Flameless combustion, computational fluid dynamics, MILD combustion, RANS simulation, Flamelet generated manifolds*

1. INTRODUCTION

The flameless combustion regime has been the subject of recent research for its potential to reduce pollutant emission (Cheong *et al.*, 2017; Khidr *et al.*, 2017; Xing *et al.*, 2017). It was noticed that the reactants temperature must be greater than the autoignition temperature to achieve the Flameless regime (Wunning and Wunning, 1997). One possible way is by recirculating the hot combustion products and mixing it with the fresh reactants (Cavaliere and de Joannon, 2004).

Experiments showed that by establishing an internal recirculation it is possible to achieve the flameless regime over a wide range of operating conditions (Rebola *et al.*, 2013b). Moreover the influence of the thermal input (Veríssimo *et al.*, 2013a) and inlet air velocity (Veríssimo *et al.*, 2013b) on the pollutant emission, temperature distribution and major species distributions were assessed experimentally. In flameless regime, the peaks in temperature are attenuated and the temperature field is more uniform in comparison to the conventional flame regime.

The onset transition from conventional flame to flameless and its fundamentals are still open questions. Direct Numerical Simulations (DNS) of premixed (Minamoto and Swaminathan, 2015), non-premixed (Göktolga *et al.*, 2015) and experimental Planar Laser Induced Fluorescence (PLIF) (Zhou *et al.*, 2017) indicate that at the flame thickness scale, the reaction still occurs in thin zones that are strongly wrinkled by turbulence in such a way that it self-interacts. This effect of turbulence combined with the dilution of the reactants with the burnt gases, results in a less intense reaction rate but present in a greater region compared with the conventional flame.

Zhou *et al.* (2017) also concluded that what makes the flame not visible is the emission reduction of the CH intermediate specie in the reaction zone. Although there are thin reaction zones, their less intense reaction rates results in smaller temperatures. Hence, NO_x production is reduced since the thermal NO formation mechanism is suppressed.

At the scale of combustion chambers, Reynolds Averaged Navier-Stokes (RANS) simulations were used to capture the flameless regime (Parente *et al.*, 2016; Aminian *et al.*, 2016; Liu *et al.*, 2015; Hosseini *et al.*, 2014). Most studies rely on the standard k-ε turbulence model and detailed chemistry with simplified chemical mechanisms and the *Eddy Dissipation Concept* for turbulence-chemistry interaction.

The flamelet generated manifold (FGM) approach is a chemical reduction mechanism that proposes to represent a complex detailed chemical mechanism using only few control variables reducing drastically the computational time. It has been developed to model premixed flames (Oijen and Goey, 2000; Van Oijen *et al.*, 2007), adapted to non premixed and partially premixed cases (Vreman *et al.*, 2008; Nguyen *et al.*, 2010) and extended to include heat loss effects (Donini *et al.*, 2017).

The objective of this work is to investigate the influence of turbulence by means of the turbulent kinetic energy and

Kolmogorov time scales present on three experimental cases studied by Zhou *et al.* (2017), namely flameless, transition and conventional flame regimes. The influence of different operating conditions on the turbulence fields and in the turbulence-chemistry interaction are the focus of the results.

2. METHODOLOGY

The computational domain is based on the geometry described by Veríssimo *et al.* (2013b). An axisymmetric two-dimensional domain was used for the numerical simulations. Pure methane and air are considered as fuel and oxidant respectively. Fuel inlet diameter is 2 mm and air inlet diameter is 10 mm. Figure 1 and figure 2 show the numerical domain dimensions and its boundary names respectively.

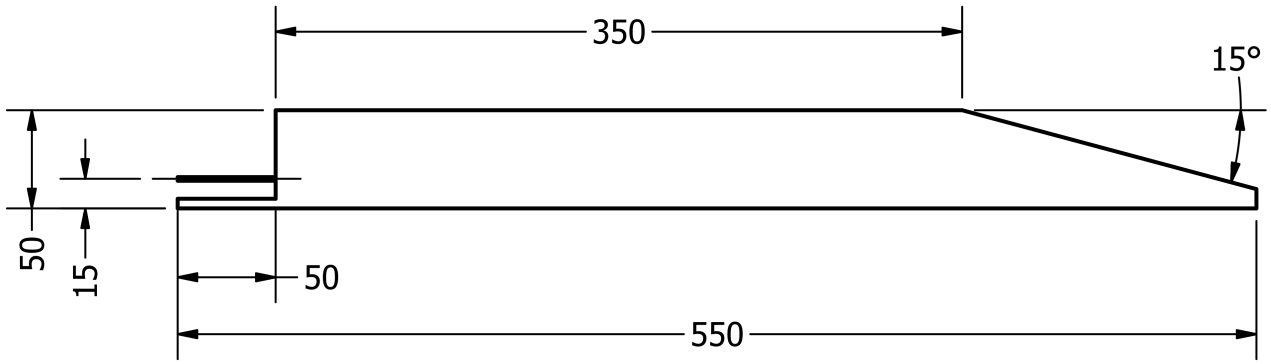

Figure 1. Computational domain dimensions in mm.

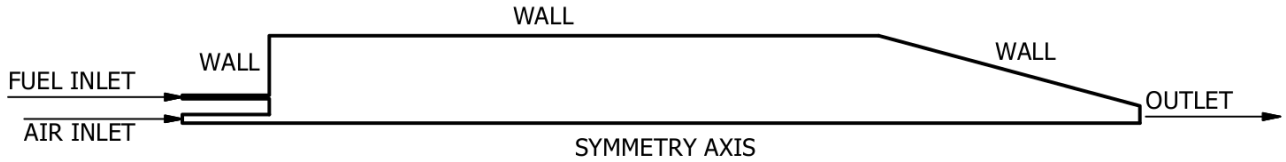

Figure 2. Computational domain with boundary conditions.

Three cases with different equivalence ratios were calculated. Flameless $\phi = 0.91$, transition $\phi = 0.67$ and conventional flame $\phi = 0.53$. For all cases, the mean fuel inlet velocity was 6 m/s as in Zhou *et al.* (2017). For all walls, the velocity was set to zero and the mesh was refined so the Y^+ is less than 5 for all cases. Heat transfer through the walls is estimated for a 30 mm thick thermal insulation as in Zhou *et al.* (2017) resulting in a heat transfer coefficient of 6.6 W/m^2K. The turbulent kinetic energy and turbulent dissipation rate fields boundary conditions are estimated for a turbulence intensity of 6% and the length scale of the respective inlet. A length of 5 air inlet diameters was used at the inlets to minimize the numerical effects of the boundary conditions.

The pressure-based solver was applied with coupled pressure-velocity approach. Pseudo-transient settings was used for robustness to achieve a steady-state solution. Monitor points for temperature indicated the simulation reached a steady-state solution after 5000 iterations. Second order discretization schemes were chosen for all operators. For advective terms the Second Order Upwind scheme was applied and gradients were discretized using the Least Squares Cell Based scheme.

Rebola *et al.* (2013a) evaluated the performance of several turbulence models for the flameless combustion regime. In agreement with the authors conclusions, the standard k-ε model was applied in this work since it demonstrated to perform better in this case. Radiation effect was accounted using the discrete ordinates method with the weighted-sum-of-gray-gases model for the radiative properties.

The FGM chemistry reduction technique was used for the account of chemical kinetics. Premixed flamelets were used for generation of the FGM table with the GRI3.0 chemical kinetics mechanism. The total enthalpy H is considered along with the mixture fraction Z and progress variable $\mathcal{Y}$ as a control variable of the FGM table to account for the heat transfer through the chamber walls. The turbulence-chemistry interaction was modeled by the presumed β-PDF approach in which a FGM manifold is created performing a convolution of the FGM table with the β shaped probability density functions of the mixture fraction Z and progress variable $\mathcal{Y}$. The variance of mixture fraction $Z^{"2}$ and progress variable $\mathcal{Y}^{"2}$ distributions were calculated via their transport equations during CFD run-time for composition of their respective β-PDFs. Apart from continuity, momentum, k and ε the transport equations solved for the FGM model are (ANSYS

Fluent, version 17.1)

$$\frac{\partial}{\partial t}\left(\rho\overline{Z}\right)+\frac{\partial}{\partial x_i}\left(\rho\bar{u}_i\overline{Z}\right)=\frac{\partial}{\partial x_i}\left[\left(\frac{k}{c_P}+\frac{\mu_t}{Pr_t}\right)\frac{\partial\overline{Z}}{\partial x_i}\right] \tag{1}$$

$$\frac{\partial}{\partial t}\left(\rho\overline{Z^{"2}}\right)+\frac{\partial}{\partial x_i}\left(\rho\bar{u}_i\overline{Z^{"2}}\right)=\frac{\partial}{\partial x_i}\left[\left(\frac{k}{c_P}+\frac{\mu_t}{Pr_t}\right)\frac{\partial\overline{Z^{"2}}}{\partial x_i}\right]+C_g\mu_t\frac{\partial\bar{Z}}{\partial x_i}\frac{\partial\bar{Z}}{\partial x_i}-C_d\rho\frac{\varepsilon}{k}\overline{Z^{"2}} \tag{2}$$

$$\frac{\partial}{\partial t}\left(\rho\overline{\mathcal{Y}}\right)+\frac{\partial}{\partial x_i}\left(\rho\bar{u}_i\overline{\mathcal{Y}}\right)=\frac{\partial}{\partial x_i}\left[\left(\frac{k}{c_P}+\frac{\mu_t}{Sc_t}\right)\frac{\partial\overline{\mathcal{Y}}}{\partial x_i}\right]+\overline{\dot{w}}_{\mathcal{Y}} \tag{3}$$

$$\frac{\partial}{\partial t}\left(\rho\overline{\mathcal{Y}^{"2}}\right)+\frac{\partial}{\partial x_i}\left(\rho\bar{u}_i\overline{\mathcal{Y}^{"2}}\right)=\frac{\partial}{\partial x_i}\left[\left(\frac{k}{c_P}+\frac{\mu_t}{Sc_t}\right)\frac{\partial\overline{\mathcal{Y}^{"2}}}{\partial x_i}\right]+C_\phi\frac{\mu_t}{Sc_t}\frac{\partial\bar{\mathcal{Y}}}{\partial x_i}\frac{\partial\bar{\mathcal{Y}}}{\partial x_i}-C_\phi\rho\frac{\varepsilon}{k}\overline{\mathcal{Y}^{"2}} \tag{4}$$

$$\frac{\partial}{\partial t}\left(\rho\overline{H}\right)+\frac{\partial}{\partial x_i}\left(\rho\bar{u}_i\overline{H}\right)=\frac{\partial}{\partial x_i}\left[\left(\frac{k}{c_P}+\frac{\mu_t}{Pr_t}\right)\frac{\partial\overline{H}}{\partial x_i}\right]+\overline{\dot{w}}_{radiation} \tag{5}$$

in which $Pr_t = 0.85$, $Sc_t = 0.7$, $C_d = 2.0$, $C_g = 2.86$, $C_\phi = 2.0$ and the source term for the progress variable is $\overline{\dot{w}}_{\mathcal{Y}} = \int\int \dot{w}_{\mathcal{Y}}(\mathcal{Y},H,Z)P(\mathcal{Y},\overline{\mathcal{Y}},\overline{\mathcal{Y}^{"2}})P(Z,\overline{Z},\overline{Z^{"2}})\ \mathrm{d}\mathcal{Y}\,\mathrm{d}Z$

The thermochemical properties and all 53 species present in the chemical kinetics mechanism are retrieved from the FGM manifold via linear interpolations through the five control variables.

Cases were calculated in the sequence flameless, transition and conventional flame. Transition and conventional flame cases were initialized with its previous case solution. Since the fuel inlet velocity was constant in all cases, the air mass flow rate at the inlet was parameterized in order to simulate the three equivalence ratio cases. The flameless case was initialized with the solution of a non reacting steady-state case for its final reactive solution. The combustion models were ignited assigning unity value for the progress variable in the rectangle region $[(0,0)\ (0.150,0.025)]$.

3. RESULTS

Veríssimo *et al.* (2013b) observed that the recirculation zone size and position do not alter considerably by varying the mean air inlet velocity and the experimental results were carried only for cases of non reacting flow. However, figure 3 illustrates the streamlines for the three calculated cases under reacting flow conditions.

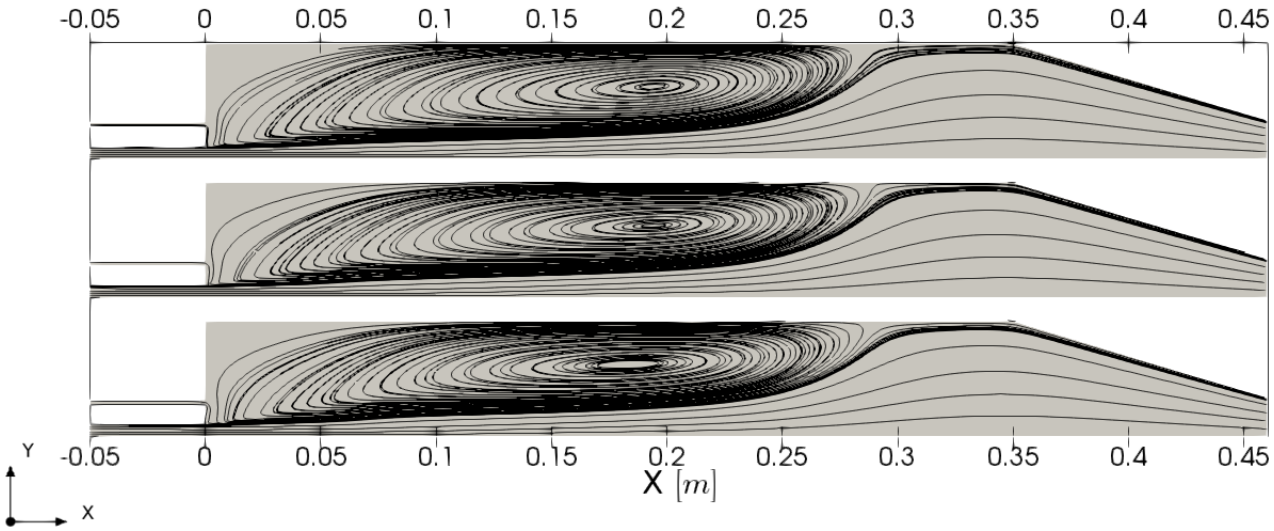

Figure 3. Recirculation zone size and position for the three cases. Flameless bottom, transition middle and conventional flame top.

The experimental conclusion regarding the position and size of the recirculation zone can be observed from the numerical results in figure 3 for the reactive flow field. For all cases, the hot combustion products recirculate and mix with the fresh reactants. This indicates that the proposed numerical methodology is able to capture one important characteristic of the flow field in the flameless combustion chamber in study.

Figure 4 shows the magnitude of the velocity field for the three calculated cases. It is clear that for all cases, the main recirculation structure is determined by the central jet since it presents the highest velocities, consequently high

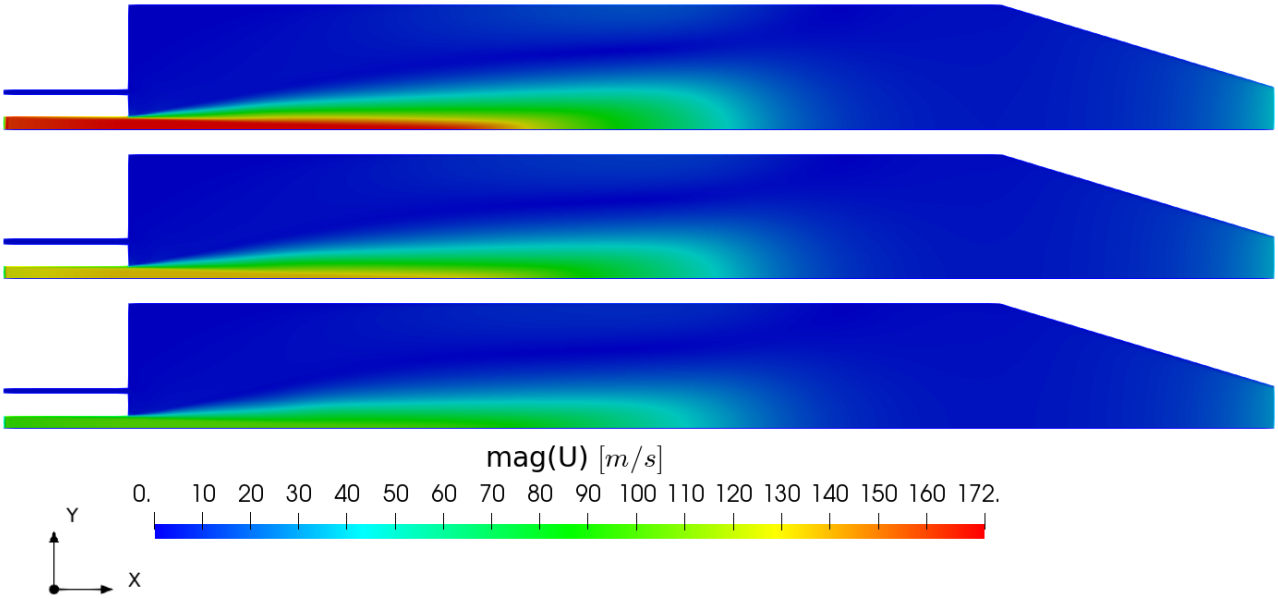

Figure 4. Recirculation zone size and position for the three cases. Flameless bottom, transition middle and conventional flame top.

momentum, at the inlet area. The fuel jet, due to its lower momentum, is carried by the recirculating fluid in the direction of the air jet, originating the air-fuel mixing region.

Figure 5 shows the turbulent kinetic energy field. It is observable that with an increase in the air inlet velocity, the turbulent kinetic energy field increases also near the air-fuel mixing region. This indicates that the flameless regime takes place in a less intense turbulent flow field compared to the transition and conventional flame regimes studied.

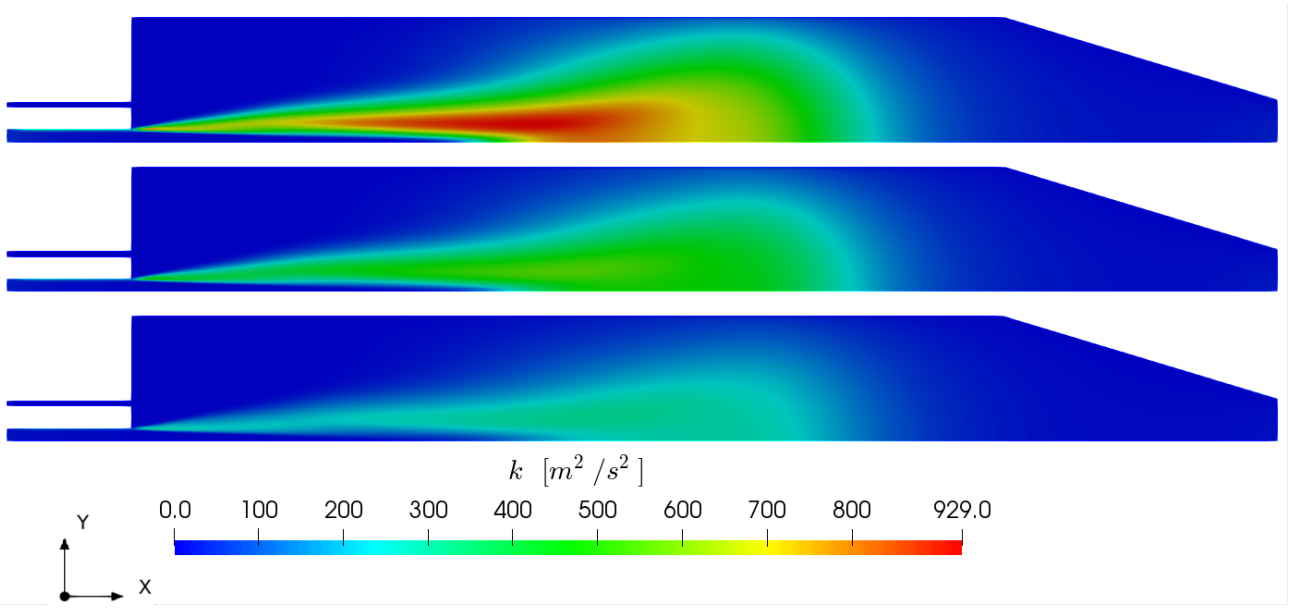

Figure 5. Turbulent kinetic energy field k for the three cases. Flameless bottom, transition middle and conventional flame top.

Several scales are present in a turbulent flow according to Kolmogorov's energy cascade theory. The smallest scales are known as Kolmogorov scales and the largest as integral scales. The Kolmogorov time scale may be defined as $t_\eta = (\nu/\varepsilon)^{1/2}$ (Pope, 2001). Figure 6 shows the Kolmogorov time scale distribution throughout the flameless chamber. It was noticed that smaller Kolmogorov time scales occupy a smaller region in the flameless case which indicates a less intense turbulent flow.

In turbulent combustion, the turbulence-chemistry interaction is imperative to characterize the phenomenon which is not only dependent on turbulence but also from the chemical kinetics. One dimensionless parameter relating turbulence with chemical kinetics, developed in the context of premixed flames, is the Damköhler Da number. Although the

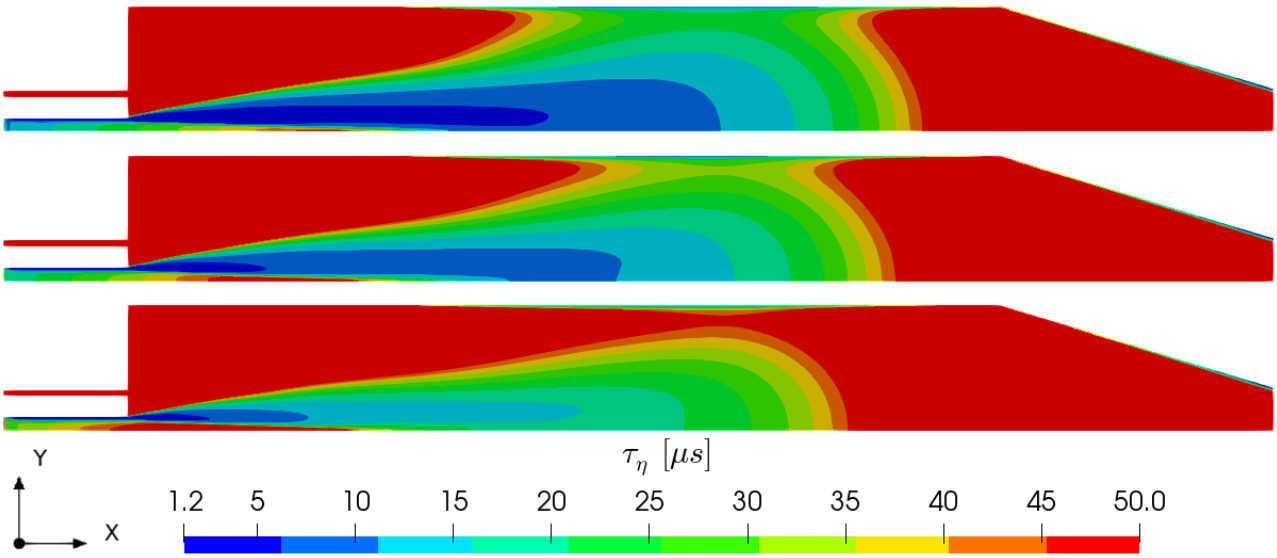

Figure 6. Kolmogorov time scale distribution τ_η for the three cases. Flameless bottom, transition middle and conventional flame top.

cases simulated in this study are highly complex and its fundamental flame structure is still a subject of discussion, the Damköhler number will be used to drive some qualitative conclusions comparing the three cases.

The Damköhler number is defined as $Da = t_0/t_c$ in which t_0 is the turbulence integral time scale and t_c the chemistry time scale, here estimated as $t_0 = k/\varepsilon$ and $t_c = \alpha/s_L^2$ in which α is the thermal diffusivity and s_L is the laminar flame speed. k and ε are results calculated from the turbulence model and α and s_L where retrieved from the FGM manifold.

Figure 7 illustrates the distribution of the Damköhler number inside the combustion chamber for the three cases. It can be seen that, on the conventional flame case, the Damköhler number is less than 0.2 in most part of the chamber, indicating that the chemistry time scale is higher than the most energetic turbulent eddies. This may imply that turbulence has a weak interaction with the flame. The opposite is observable on flameless case. In most part of the chamber, the Damköhler number is of the order of one and so the turbulent large scales are of the same order than the chemistry scale. It also implies that turbulence interacts more with the chemical kinetics in this case and this interaction may result in the transition from conventional flame case to the flameless combustion regime.

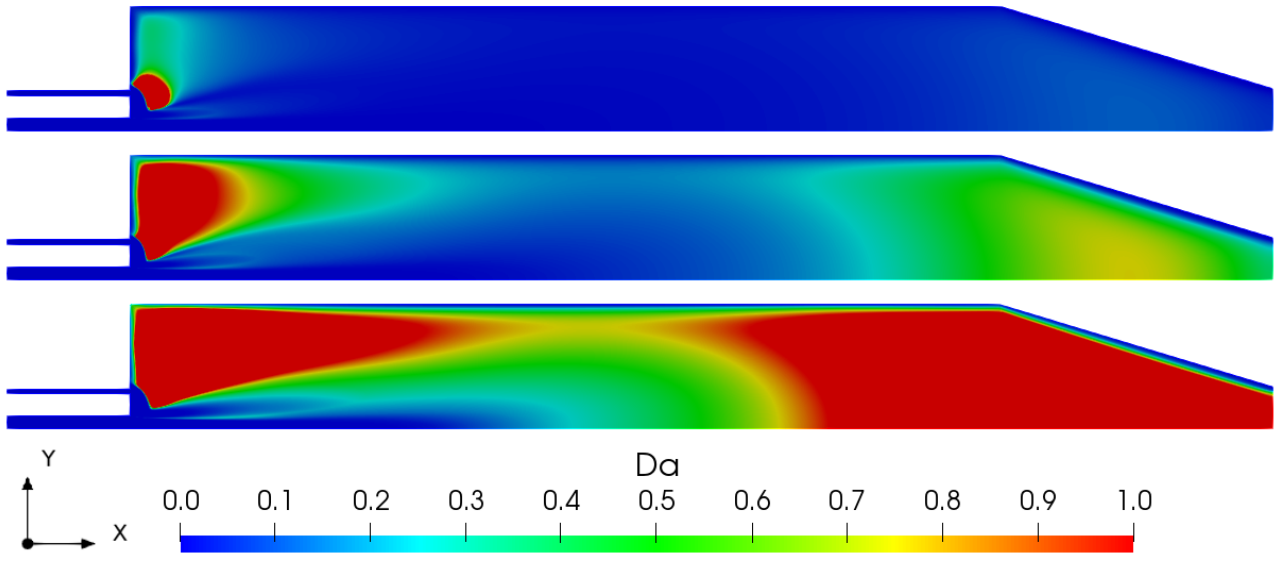

Figure 7. Damköhler number Da distribution for the three cases. Flameless bottom, transition middle and conventional flame top.

Another well reported characteristic of the flameless regime is the smooth temperature distribution throughout the chamber (Wunning and Wunning, 1997; Cavaliere and de Joannon, 2004; Lamouroux *et al.*, 2014; Parente *et al.*, 2016).

Figure 8 presents the temperature distributions inside the chamber for the three cases. It can be observed that for the flameless case, smaller temperature gradients are present in the flow and it is not possible to clearly determine a small region where the chemical reactions are taking place as it is possible for the conventional case.

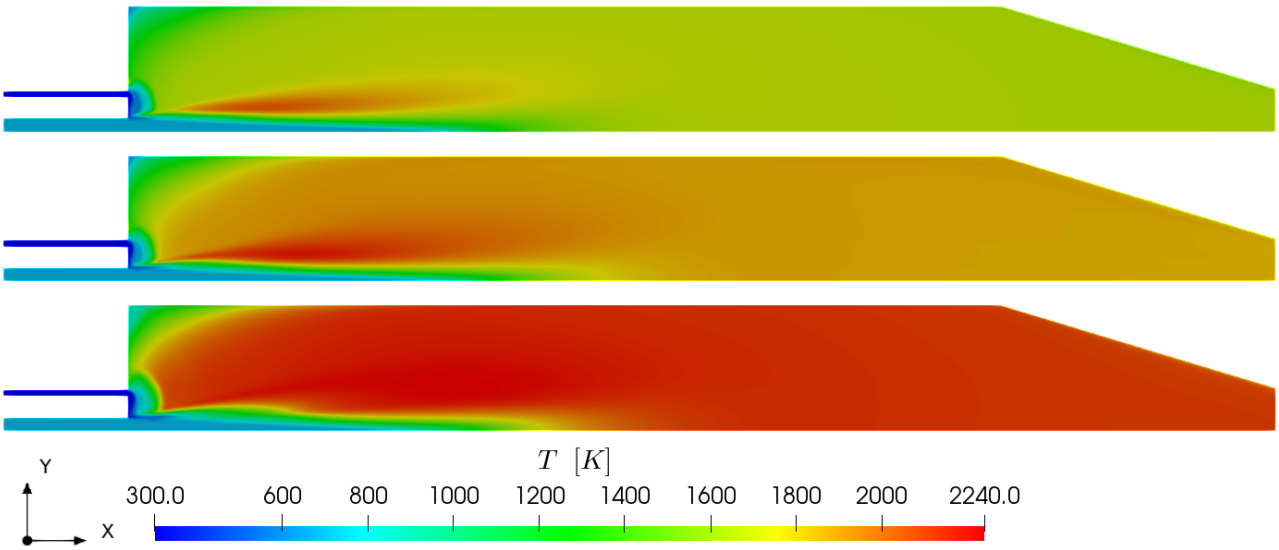

Figure 8. Temperature field T for the three cases. Flameless bottom, transition middle and conventional flame top.

Although the temperature distribution behaviour is in accordance with experimental evidence in literature, the values are overestimated specially for the flameless case in which temperatures are close to the adiabatic flame temperature of 2266 K for this case. In tabulated chemistry approaches such as the FGM, it was recently argued that for cases with high dilution of the reactants, including the dilution level as another control variable, results in better prediction of the chemistry behaviour of the reactive flow since dilution is accounted on the generation of the FGM tables (Lamouroux *et al.*, 2014). The implementation and assessment of this methodology in the OpenFOAM CFD package is currently been done by our research group.

4. CONCLUSIONS

The proposed numerical methodology was able to predict important characteristics of the flow field of the flameless combustion regime discussed in Veríssimo *et al.* (2013b). The size and position of the recirculation zone inside the combustion chamber do not alter considerably by increasing the air inlet velocity as observed experimentally for non reactive cases. The low momentum of the fuel inlet jet along with the recirculating combustion products results in air-fuel-products mixing before the combustion process region in all cases.

Turbulent kinetic energy presents similar distributions for all cases with lower values for the flameless case compared with the conventional flame case. Also, smaller Kolmogorov time scales occupy a smaller region of the flow on the flameless case indicating a less intense turbulent flow compared with the conventional flame case due to their respective lowest and highest air mass flow.

Interaction of turbulence with the chemical kinetics was assessed through the estimation of the Damköhler number distribution inside the combustion chamber for all cases. It may indicate that although turbulence is less intense for the flameless case, the turbulent large scales interact more with the chemical kinetics. This interaction may be responsible for the transition from conventional flame to flameless combustion regime.

Temperature distributions inside the chamber reproduced the experimental observations of smaller temperature gradients for the flameless case compared with the conventional flame, but, the numerical models overestimate the values specially for the flameless case.

Implementation and assessment of particular strategies for numerical modelling of flameless combustion is under development by our research group along with experimental studies to validate the numerical models and better understand the processes involved on flameless combustion.

5. ACKNOWLEDGEMENTS

The authors would like to acknowledge Escola Politécnica da Universidade de São Paulo, Fundação de Amparo à Pesquisa do Estado de São Paulo (FAPESP) project number FAPESP 2013/50238-3, FAPESP 2014/50279-4 and Conselho Nacional de Desenvolvimento Cientifico e Tecnológico (CNPq) for the research support.

6. REFERENCES

Aminian, J., Galletti, C. and Tognotti, L., 2016. "Extended EDC local extinction model accounting finite-rate chemistry for MILD combustion ". *Fuel*, Vol. 165, pp. 123 – 133.

ANSYS Fluent, version 17.1. *(2016) Theory Guide*.

Cavaliere, A. and de Joannon, M., 2004. "Mild combustion". *Progress in Energy and Combustion Science*, Vol. 30, pp. 329 – 366.

Cheong, K.P., Li, P., Wang, F. and Mi, J., 2017. "Emissions of NO and CO from counterflow combustion of CH4 under MILD and oxyfuel conditions". *Energy*, Vol. 124.

Donini, A., Bastiaans, R., van Oijen, J. and de Goey, L., 2017. "A 5-d implementation of fgm for the large eddy simulation of a stratified swirled flame with heat loss in a gas turbine combustor". *Flow, Turbulence and Combustion*, Vol. 98, No. 3, pp. 887–922.

Göktolga, M.U., van Oijen, J.A. and de Goey, L.P.H., 2015. "3D DNS of MILD combustion: A detailed analysis of heat loss effects, preferential diffusion, and flame formation mechanisms ". *Fuel*, Vol. 159, pp. 784 – 795.

Hosseini, S.E., Bagheri, G. and Wahid, M.A., 2014. "Numerical investigation of biogas flameless combustion". *Energy Conversion and Management*, Vol. 81, pp. 41 – 50.

Khidr, K.I., Eldrainy, Y.A. and EL-Kassaby, M.M., 2017. "Towards lower gas turbine emissions: Flameless distributed combustion".

Lamouroux, J., Ihme, M., Fiorina, B. and Gicquel, O., 2014. "Tabulated chemistry approach for diluted combustion regimes with internal recirculation and heat losses". *Combustion and Flame*, Vol. 161, pp. 2120 – 2136.

Liu, B., Wang, Y.H. and Xu, H., 2015. "Mild combustion in forward flow furnace of refinery-off gas for low-emissions by deflector". *Applied Thermal Engineering*, Vol. 91, pp. 1048 – 1058.

Minamoto, Y. and Swaminathan, N., 2015. "Subgrid scale modelling for mild combustion". *Proceedings of the Combustion Institute*, Vol. 35, pp. 3529 – 3536.

Nguyen, P.D., Vervisch, L., Subramanian, V. and Domingo, P., 2010. "Multidimensional flamelet-generated manifolds for partially premixed combustion". *Combustion and Flame*, Vol. 157, No. 1, pp. 43–61.

Oijen, J.V. and Goey, L.D., 2000. "Modelling of Premixed Laminar Flames using Flamelet-Generated Manifolds". *Combustion Science and Technology*, Vol. 161, No. May 2016, pp. 113–137.

Parente, A., Malik, M.R., Contino, F., Cuoci, A. and Dally, B.B., 2016. "Extension of the Eddy Dissipation Concept for turbulence/chemistry interactions to MILD combustion ". *Fuel*, Vol. 163, pp. 98 – 111.

Pope, S.B., 2001. "Turbulent flows".

Rebola, A., Coelho, P. and Costa, M., 2013a. "Assessment of the performance of several turbulence and combustion models in the numerical simulation of a flameless combustor". *Combustion Science and Technology*, Vol. 185, No. 4, pp. 600–626.

Rebola, A., Costa, M. and Coelho, P.J., 2013b. "Experimental evaluation of the performance of a flameless combustor". *Applied Thermal Engineering*, Vol. 50, pp. 805–815.

Van Oijen, J.A., Bastiaans, R.J.M. and De Goey, L.P.H., 2007. "Low-dimensional manifolds in direct numerical simulations of premixed turbulent flames". *Proceedings of the Combustion Institute*, Vol. 31 I, pp. 1377–1384.

Veríssimo, A., Rocha, A. and Costa, M., 2013a. "Experimental study on the influence of the thermal input on the reaction zone under flameless oxidation conditions". *Fuel Processing Technology*, Vol. 106, pp. 423–428.

Veríssimo, A., Rocha, A. and Costa, M., 2013b. "Importance of the inlet air velocity on the establishment of flameless combustion in a laboratory combustor". *Experimental Thermal and Fluid Science*, Vol. 44, pp. 75 – 81.

Vreman, A., Albrecht, B., van Oijen, J., de Goey, L. and Bastiaans, R., 2008. "Premixed and nonpremixed generated manifolds in large-eddy simulation of sandia flame d and f". *Combustion and Flame*, Vol. 153, No. 3, pp. 394 – 416.

Wunning, J. and Wunning, J., 1997. "Flameless oxidation to reduce thermal NO-formation ". *Progress in Energy and Combustion Science*, Vol. 23, pp. 81 – 94.

Xing, F., Kumar, A., Huang, Y., Chan, S., Ruan, C., Gu, S. and Fan, X., 2017. "Flameless combustion with liquid fuel: A review focusing on fundamentals and gas turbine application". *Applied Energy*, Vol. 193, pp. 28–51.

Zhou, B., Costa, M., Li, Z., Aldén, M. and Bai, X.S., 2017. "Characterization of the reaction zone structures in a laboratory combustor using optical diagnostics: From flame to flameless combustion". *Proceedings of the Combustion Institute*, Vol. 36, pp. 4305–4312.

7. RESPONSIBILITY NOTICE

The authors are the only responsible for the printed material included in this paper.